molecules

MDPI

Article

Synthesis of Disubstituted Carboxonium Derivatives of *Closo*-Decaborate Anion $[2,6\text{-}B_{10}H_8O_2CC_6H_5]^-$: Theoretical and Experimental Study

Ilya N. Klyukin [1,*], Anastasia V. Kolbunova [1], Alexander S. Novikov [2,3,*], Alexey V. Nelyubin [1], Andrey P. Zhdanov [1], Alexey S. Kubasov [1], Nikita A. Selivanov [1], Alexander Yu. Bykov [1], Konstantin Yu. Zhizhin [1] and Nikolay T. Kuznetsov [1]

[1] Kurnakov Institute of General and Inorganic Chemistry, Russian Academy of Sciences, Leninskii Pr. 31, 117907 Moscow, Russia
[2] Institute of Chemistry, Saint Petersburg State University, Universitetskaya nab. 7–9, 199034 Saint Petersburg, Russia
[3] Research Institute of Chemistry, Peoples' Friendship University of Russia (RUDN University), Miklukho-Maklaya St. 6, 117198 Moscow, Russia
* Correspondence: klukinil@igic.ras.ru (I.N.K.); a.s.novikov@spbu.ru (A.S.N.)

Abstract: A comprehensive study focused on the preparation of disubstituted carboxonium derivatives of *closo*-decaborate anion $[2,6\text{-}B_{10}H_8O_2CC_6H_5]^-$ was carried out. The proposed synthesis of the target product was based on the interaction between the anion $[B_{10}H_{11}]^-$ and benzoic acid C_6H_5COOH. It was shown that the formation of this product proceeds stepwise through the formation of a mono-substituted product $[B_{10}H_9OC(OH)C_6H_5]^-$. In addition, an alternative one-step approach for obtaining the target derivative is postulated. The structure of tetrabutylammonium salts of carboxonium derivative $((C_4H_9)_4N)[2,6\text{-}B_{10}H_8O_2CC_6H_5]$ was established with the help of X-ray structure analysis. The reaction pathway for the formation of $[2,6\text{-}B_{10}H_8O_2CC_6H_5]^-$ was investigated with the help of density functional theory (DFT) calculations. This process has an electrophile induced nucleophilic substitution (EINS) mechanism, and intermediate anionic species play a key role. Such intermediates have a structure in which one boron atom coordinates two hydrogen atoms. The regioselectivity for the process of formation for the 2,6-isomer was also proved by theoretical calculations. Generally, in the experimental part, the simple and available approach for producing disubstituted carboxonium derivative was introduced, and the mechanism of this process was investigated with the help of theoretical calculations. The proposed approach can be applicable for the preparation of a wide range of disubstituted derivatives of *closo*-borate anions.

Keywords: *closo*-borates; carboxonium derivatives; reaction mechanism; QTAIM; DFT

check for updates

Citation: Klyukin, I.N.; Kolbunova, A.V.; Novikov, A.S.; Nelyubin, A.V.; Zhdanov, A.P.; Kubasov, A.S.; Selivanov, N.A.; Bykov, A.Y.; Zhizhin, K.Y.; Kuznetsov, N.T. Synthesis of Disubstituted Carboxonium Derivatives of *Closo*-Decaborate Anion $[2,6\text{-}B_{10}H_8O_2CC_6H_5]^-$: Theoretical and Experimental Study. *Molecules* **2023**, *28*, 1757. https://doi.org/10.3390/molecules28041757

Academic Editors: Aurora Costales and Fernando Cortés-Guzmán

Received: 29 December 2022
Revised: 9 February 2023
Accepted: 9 February 2023
Published: 13 February 2023

Copyright: © 2023 by the authors. Licensee MDPI, Basel, Switzerland. This article is an open access article distributed under the terms and conditions of the Creative Commons Attribution (CC BY) license (https://creativecommons.org/licenses/by/4.0/).

1. Introduction

Molecular modelling enables the study of the main features of chemical compounds in a clear and simple way [1–5]. Geometric parameters, chemical bonding, atomic charges, electrostatic potential and many other phenomena can be analyzed quickly and with great accuracy [6–10]. In addition, many methods have been developed for the investigation of the reactivity of molecules and reaction mechanisms [11–13]. Utilizing the methods of quantum chemistry, it is possible to investigate potential energy surface and study intermediates and transition states of various reactions [14–16]. Methods such as QTAIM (Quantum Theory of Atoms in Molecules), NBO (Natural Bond Orbitals) and ELF (Electron Localization Function) enable the definition of peculiarities in the electronic structure of key intermediates and transition states [17–21]. Conceptual DFT enables an evaluation of the electrophile/nucleophile nature of a chemical system through merely estimating the energy of HOMO/LUMO orbitals [22–26]. Thus, molecular modelling is a powerful tool for examining the chemical transformation of molecules.

All previously mentioned methods and approaches are very applicable for boron cluster compounds such as *closo*-borates, carboranes and metallocarboranes [27–30]. The chemistry of *closo*-borate anions is wide and diverse [31,32]. Borylated analogues of organic compounds such as esters, nitriles and carboxylic acids play a special role in this field of chemistry [33–36]. Borylated analogues are more reactive than the original organic molecules [37]. Thus, such borylated systems can interact with a wide range of nucleophiles with the formation of different derivatives of *closo*-borate anions [38]. Derivatives of *closo*-borate anions have found different applications in medicine, catalysis and many other fields [39].

Theoretical investigations of *closo*-borate anions' reactivity were conducted, using a wide range of methods [40–42]. For example, the question "how does the reactivity of boron cluster compounds change depending on their structure?" was addressed using Conceptual DFT [43]. It was found that, with increasing boron cluster size, the nucleophilicity of boron clusters reduced [44]. In addition to the Conceptual DFT approach for some other processes, their mechanisms have been investigated in detail. The main intermediates were identified, and transition states were investigated. For example, the mechanisms of nucleophilic addition reactions to nitrile derivatives of *closo*-decaborate anions $[B_nH_{n-1}NCR]^-$ n = 10, 12, R = Alkyl, Aryl were investigated [45,46]. It was demonstrated that the stereoselectivity of the final products depends on the structure of the transition state. The main reason for this phenomena is the formation of intermolecular dihydrogen bond between the hydrogen atom of the boron cluster and the proton from the nucleophile.

The most interesting aspect of the investigation process is EINS process (Electrophile Induced Nucleophilic Substitution) [47,48]. As an electrophile inducer, various Lewis and Bronsted acids (CF_3COOH, CF_3SO_3H, BF_3*Et_2O, etc.) can be used [49–51]. Different organic molecules such as organic nitriles RCN, ethers R_2O and thioethers R_2S can be used as nucleophiles [52,53]. However, despite the widespread occurrence of EINS process in laboratory practice, its mechanism has been studied in only a few papers. The mechanism of chlorination of *closo*-borates with the HCl molecule has been investigated in several publications [54,55]. This paper reports on comprehensive investigations of the key stages of the EINS process. The process of chlorination started with the formation of a complex between anion $[B_{10}H_{10}]^{2-}$ and the HCl molecule. Then the formation of key intermediate $[B_{10}H_9H_2]^-$ was indicated. This complex undewent the process of elimination with the formation of $[B_{10}H_9]^-$ intermediate. The process of nucleophilic addition occurred, and $[2\text{-}B_{10}H_9Cl]^{2-}$ was formed. It is particularly noteworthy that regioselectivity of the process was investigated and the preference for substitution at the equatorial position of the boron cluster was proven. In addition, the EINS process was performed on the formation of a carboxylic derivative of the *closo*-borate anion with the general form $[B_{10}H_9OCOCH_3]^{2-}$ [56]. This process is based on interaction between the $[B_{10}H_{10}]^{2-}$ anion and acetic acid. At the first stage of the process, a proton from the hydroxy group of acetic acid migrated to the boron cluster cage with the formation of the $[B_{10}H_{11}]^-$ anion. Then the process of H_2 elimination occurred and the $[B_{10}H_9]^-$ intermediate was formed. Finally, this anion species interacted with the $CH3COO^-$ anion with formation of $B_{10}H_9OCOCH_3]^{2-}$.

In the present study, the main focus was on the disubstituted carboxonium derivative $[2,6\text{-}B_{10}H_8O_2CC_6H_5]^-$. This anion is a member of a class of borylated heterocycles [57]. Previously, derivatives $[2,6\text{-}B_{10}H_8O_2CR]^-$ R = CH_3, C_2H_5 were obtained by the interaction between $[B_{10}H_{11}]^-$ and acetic acid CH_3COOH [58,59]. In this work, based on the same approach, the range of disubstituted carboxonium derivatives was extended and $[2,6\text{-}B_{10}H_8O_2CC_6H_5]^-$ was obtained. The applied approach is versatile and allows to different carboxonium derivatives to be obtained in a simple way. The key step of target anion formation was analyzed using DFT calculations. The driving force of the 2,6-isomer of disubstituted carboxonium derivative formation was revealed.

2. Results and Discussion

2.1. Synthesis of $[B_{10}H_8O_2CC_6H_5]^-$

Initially, an experimental synthesis of $[B_{10}H_8O_2CC_6H_5]^-$ was performed. Synthetic methods are based on analogue protocols for $[B_{10}H_8O_2CCH_3]^-$ [60], but, during this work, some synthetic protocols were improved. Synthesis of $[B_{10}H_8O_2CCH_3]^-$ was based on the interaction of $[B_{10}H_{11}]^-$ and acetic acid CH_3COOH. Acetic acid was chosen as a solvent for synthesis performing. In this case, such a synthetic protocol is not possible because of the high melting temperature of benzoic acid C_6H_5COOH. Thus, several approaches for the preparation of this derivative were carried out.

The first synthetic route was based on interactions between $[B_{10}H_{11}]^-$ and C_6H_5COOH. This process occurred in a dichloromethane CH_2Cl_2 solution at boiling point temperature (41 °C). In the first stage of this process, mono-substituted derivatives of the general form $[B_{10}H_9OC(OH)C_6H_5]^-$ were obtained. Progress of the process was monitored using a ^{11}B NMR spectra. The spectra of mono-substituted derivatives are identical to those of $[B_{10}H_9OC(OH)CH_3]^-$. The signal of one in an apical position lay at 2.3 ppm. The signal from another apical position appeared as a broadband signal in the range of 0.3 to −4.6 ppm. This broadening of the signal can be connected with the intramolecular interaction between a hydrogen atom of the boron cluster and a proton from the hydroxy group of organic moieties. The signal from the substituted position lay at −7.7 ppm. Signals from equatorial boron atoms lay at −23.8, −24.8 and −29.7 ppm. The isolation and purification of mono-substituted derivative is a complicated task, due to its thermal instability. Thus, it is possible to use mono-substituted derivative without additional manipulation; the evaporation of dichloromethane solution and washing with ether are enough.

At the next stage, the heating of mono-substituted derivative $[B_{10}H_9OC(OH)C_6H_5]^-$ led to intramolecular cyclisation when $[B_{10}H_8O_2CC_6H_5]^-$ was obtained. It is noteworthy that the cyclisation process was conducted in the absence of solvent. For this process, a rotary evaporator was used with an air bath oven. ^{11}B NMR spectra of $[B_{10}H_8O_2CPh]^-$ are similar to the analogous spectra of $[B_{10}H_8O_2CCH_3]^-$. A detailed analysis of the ^{11}B NMR spectra of $[B_{10}H_8O_2CCH_3]^-$ was carried out in the authors' previous work [61]. The ^{11}B NMR spectra of $[B_{10}H_8O_2CC_6H_5]^-$ had four signals: a signal at 0.0 ppm with integral intensities I = 2, corresponding to the boron atoms from equivalent substituted positions (B2, B6), a signal at −7.1 with integral intensities I = 2, corresponding to boron atoms from equivalent apical positions (B1, B10), signals from equatorial positions appearing at −17.6 (I = 2, B3, B9) and a signal at −30.0 (I = 4, B4, B5, B7, B8).

The process of obtaining $[B_{10}H_8O_2CC_6H_5]^-$ can be performed in one stage, without the separation and purification of $[B_{10}H_9OC(OH)C_6H_5]^-$. In this case, the reaction between $[B_{10}H_{11}]^-$ and C_6H_5COOH was carried out in an autoclave at 70 °C. Dichloromethane CH_2Cl_2 was also chosen as a solvent. The main advantage of a one-pot preparation of the target disubstituted product is the significant decrease in the total time required for the synthesis, compared with the two-stage approach. The overall yield of the target product is similar to the two-stage route.

The crystal structure of $((C_4H_9)_4N)[B_{10}H_8O_2CC_6H_5]$ salt was established using an X-ray diffraction experiment (Figure 1). The B_2O_2C cycle has an almost planar conformation, with torsion angles lying within the interval of 2 to 6°. The B-O bond lengths were in the range of 1.519 to 1.522 Å. The lengths of C-O bonds were quite similar, lying within the interval 1.274 to 1.288 Å. The equality of bond lengths indicates the presence of conjugation in the carboxylic group fragment. The main geometric parameters were quite similar to previously obtained data for the $[B_{10}H_8O_2CCH_3]^-$ anion. Thus, it can be concluded that the substituent nature of the organic acid fragment had a slight impact on the parameters of B-O and C-O bonds.

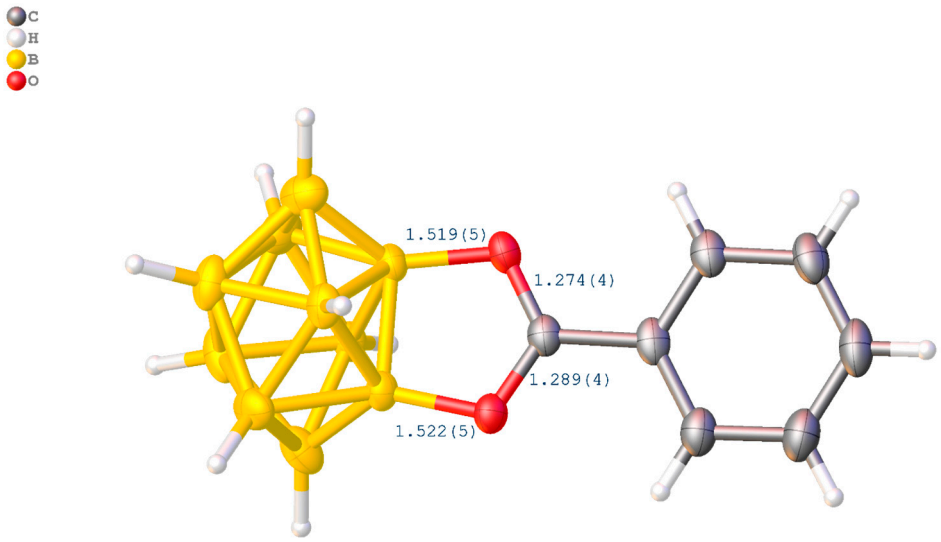

Figure 1. X-ray Structure of $[B_{10}H_8O_2CC_6H_5]^-$ anion. Length units—Å.

Several approaches to obtaining the target carboxonium derivative of the general form $[B_{10}H_8O_2CC_6H_5]^-$ have been proposed (Scheme 1, for more details also see Scheme S1). It has been shown that the formation of this product proceeds stepwise, through the formation of a mono-substituted product $[B_{10}H_9OC(OR)C_6H_5]^-$, R = H, C_2H_5. Formation of monosubstituted derivative was confirmed with the help of ^{11}B NMR spectroscopy. However, it is possible to avoid the mono derivative preparation stage and obtain the target product $[B_{10}H_8O_2CC_6H_5]^-$ in one step.

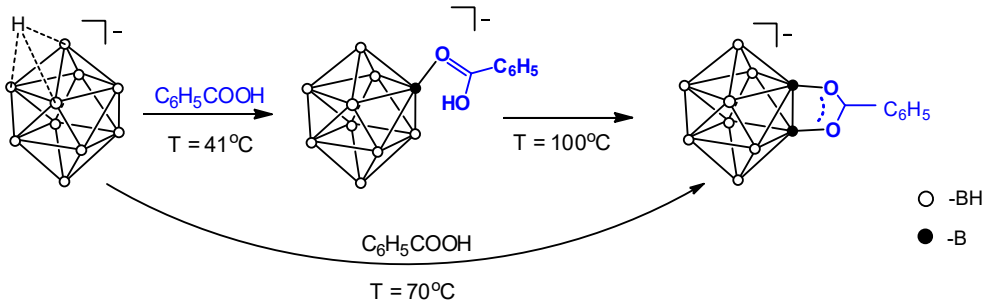

Scheme 1. General scheme of preparation of $[B_{10}H_8O_2CC_6H_5]^-$ anion.

2.2. Reaction Mechanism Investigation Based on DFT Calculations

The process of interaction between $[B_{10}H_{11}]^-$ and C_6H_5COOH was studied using DFT calculations. ωB97X-D3 was chosen as DFT functional. The given level of theory is that it is appropriate for a wide range of theoretical calculation issues such as atomic charges, chemical reactivity and covalent and non-covalent interactions [62–64]. In addition, the authors successfully used this method for the investigation of closo-borate structures, reactivity and NMR properties [46,61,65]. This mechanism study was conducted to identify the main stages of the process. It is necessary to find out the reason of regioselectivity of formation of disubstituted product. All calculations were carried out with dichlomethane CH_2Cl_2 as the solvent. The process of carboxonium derivative formation is related to the EINS process (Electrophile Induced Nucleophilic Substitution). It is well known that the initial step in the EINS process is the elimination of H_2 from the $[B_{10}H_{11}]^-$ anion, with the formation of $[B_{10}H_9]^-$ intermediate. The starting point was the calculation of the orientation complex between $[B_{10}H_{11}]^-$ and C_6H_5COOH. The structure of this orientation complex is presented below (Figure 2).

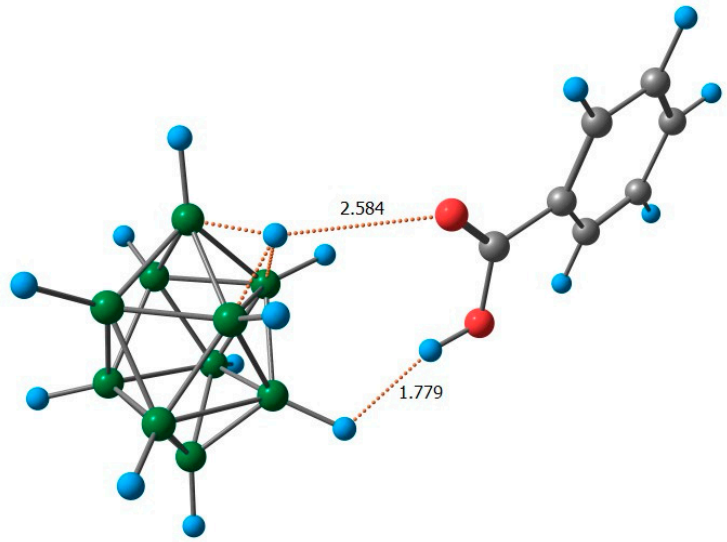

Figure 2. Structure of complex between $[B_{10}H_{11}]^-$ and C_6H_5COOH. Length units—Å, ωB97X-D3/def2-TZVPP level of theory.

However, the formation of the complex between $[B_{10}H_{11}]^-$ and C_6H_5COOH is an endergonic process. It can be concluded that, in the first stages of proton migration, the C_6H_5COOH molecule does not take part. Thus, initially, H^{fac} migrates to the equatorial boron atom with the formation of a $[B_{10}H_9(H_2)]^-$ anion. The formation of $[B_{10}H_9(H_2)]^-$ occurred through the formation of a transition state. This transition state has a structure in which one boron atom coordinates with dihydrogen, H_2. The distance between the boron atom and the hydrogen atom was equal to 1.35 Å, the distance between the hydrogen atoms in the H_2-fragment was equal to 0.86 Å and the energy barrier of the transition state was equal to 59 kJ/mol. The overall process of proton migration was endergonic, and Gibbs energy of the isomerization reaction was 30 kJ/mol (Figure 3). This anion, as in the case of the transition state, had a structure in which one boron atom coordinated with the molecule of dihydrogen, H_2. The distance between the boron atom and the hydrogen atom was equal to 1.30 Å, while the distance between the hydrogen atoms in the H_2-fragment was equal to 0.86 Å. Thus, compared with the transition state structure, the B-H bond length increased, and the H-H contact length decreased.

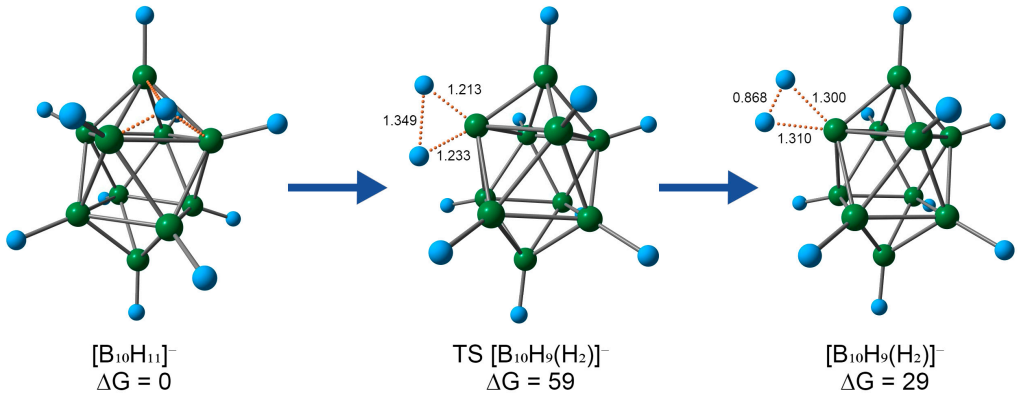

Figure 3. Isomerization process of $[B_{10}H_{11}]^-$ to $[B_{10}H_9(H_2)]^-$. Length units—Å, energy units—kJ/mol, ωB97X-D3/def2-TZVPP level of theory.

The structure of $[B_{10}H_9(H_2)]^-$ was investigated using QTAIM analysis (Figure 4). The bond path between the boron atom and the H_2 fragment was indicated in the molecular graph of electron density distribution. The main descriptors of electron density at the bond critical point (bcp) corresponding to the interaction between the boron atom and H_2 were

analyzed. The value of ρ *(r)* was equal to 0.126 e Å^{-3}, the Laplacian of electron density was equal to 0.350 e Å^{-5}, the total energy at the bcp was equal to −0.097 h e^{-1} and the delocalization index was equal to 0.342. In the contour line map of the Laplacian of electron density for the B–(H_2) fragment, the charge delocalization between boron atom and two hydrogen atoms was observed.

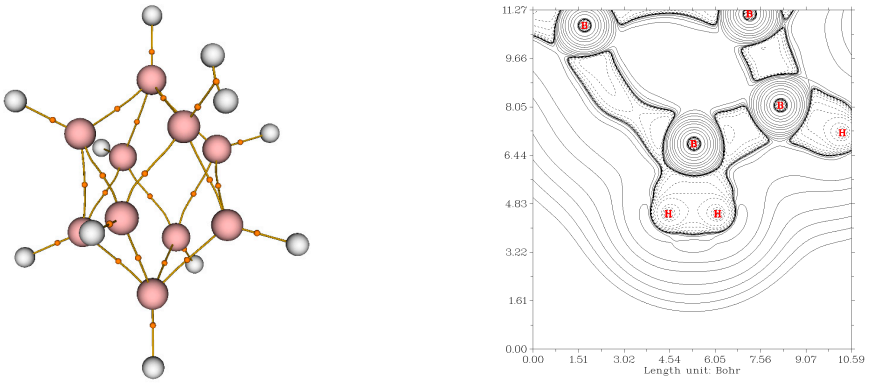

Figure 4. Molecular graph showing the results of the topological analysis of the electron density distribution in the model structure of the $[B_{10}H_9(H_2)]^-$; Contour line map of the Laplacian of electron density for B–(H_2) fragment, ωB97X-D3/def2-TZVPP level of theory.

$[B_{10}H_9(H_2)]^-$ underwent the H_2 elimination process, which is endergonic; Gibbs energy ΔG of this process was 49 kJ/mol. Thus, anion $[B_{10}H_9]^-$ was formed. Anion $[B_{10}H_9]^-$ is a short-lived intermediate with a vacant orbital on the boron atom. There are two available options of the reaction course. The first one is protonation of the *closo*-borate intermediate with the proton of the hydroxy group of benzoic acid, but this process seems to be unrealistic due to its high endergonicity. Thus, the $[B_{10}H_9]^-$ interacts with C_6H_5COOH without an activation energy barrier, with the formation of $[B_{10}H_9OC(OH)C_6H_5]^-$. The process of the formation of the mono-substituted derivative was exergonic, and Gibbs energy of the reaction between $[B_{10}H_9]^-$and C_6H_5COOH was equal to −118 kJ/mol. The overall exergonic character of the reaction between $[B_{10}H_9]^-$ and benzoic acid C_6H_5COOH due to the formation of an *exo*-polyhedral B-O bond and the instability of $[B_{10}H_9]^-$ being the main driving force of the formation of monosubstituted derivative is favorable.

The structure of $[B_{10}H_9OC(OH)C_6H_5]^-$ was analyzed (Figure 5). Experimentally, the structure of this particle was established only by ^{11}B–NMR spectroscopy data. Using theoretical modeling, the data on the structure of this derivative have been supplemented. The organic substituent can rotate freely, relative to the cluster fragment. The rotation barrier of the organic fragment was ~8 kJ/mol. The two lowest energy isomers were localized on the potential energy surface, and the difference in Gibbs energy between them was 3 kJ/mol. The structures of these isomers were stabilized with the formation of an intramolecular dihydrogen bond between the proton of the hydroxy group of the organic substituent and hydrogen from the boron cluster. The B-O bond length was equal to 1.50 Å. The bond length of the C = O bond was equal to 1.25 Å, which was longer than in the case of initial benzoic acid (1.20 Å), whereas the bond length of the C-O bond was equal to 1.29, which was shorter than that of benzoic acid (1.33 Å).

At the next step, the proton from the hydroxy group migrated to the boron cluster. This process occurred without the formation of a transition state. $[B_{10}H_9OC(O)C_6H_5{*}H^{fac}]^-$ was formed. The process of proton migration from the oxygen atom to the cluster cage was endergonic. As in the case of $[B_{10}H_9OC(OH)C_6H_5]^-$, the given anion can have different isomers. The proton atom can be localized on different shapes of the boron cluster. The difference between two isomers is less than 1 kJ/mol based on the DFT calculations at the ωB97X-D3/def2-TZVPP level of theory (see Section 3.5. Computational details). Previously, the authors investigated an analogous protonated structure, for $[B_{10}H_8O_2CCH_3{*}H^{fac}]^-$. H^{fac} is mainly bonded with apical boron atoms. In the case of $[B_{10}H_9OC(O)C_6H_5{*}H^{fac}]^-$,

the length of H^{fac}–B_{ap} was equal to 1.30 Å and H^{fac}–B_{eq} was equal to 1.44 to 1.48 Å. Given geometry parameters are also indicate that, in case of $[B_{10}H_8O_2CCH_3{*}H^{fac}]^-$, H^{fac} was predominantly bonded with the apical boron atom.

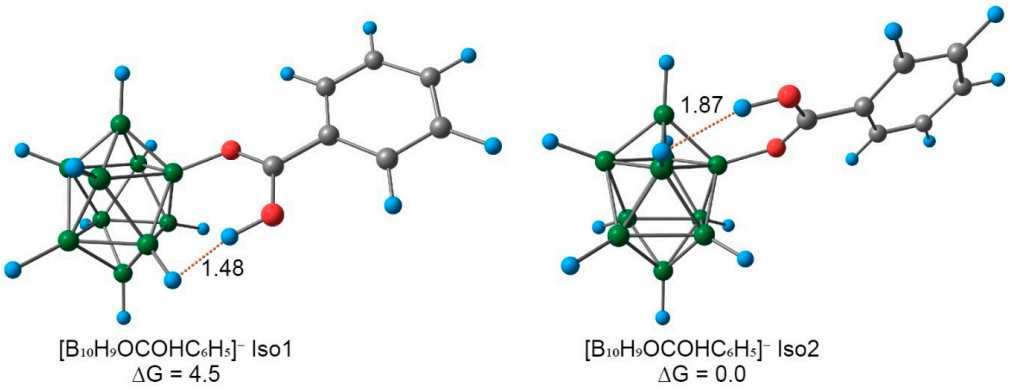

Figure 5. The structure of main isomers of $[B_{10}H_9OC(OH)C_6H_5]^-$ anion. Length units—Å, energy units—kJ/mol, ωB97X-D3/def2-TZVPP level of theory.

H^{fac} migrated with the formation of intermediate $[B_{10}H_8OC(O)C_6H_5(H_2)]^-$ (Figure 6). The process of proton migration was endergonic and, as in the case of $[B_{10}H_9(H_2)]^-$, took place through the formation of transition states. The energy barrier of transition states lay within the range 4 to 5 kJ/mol. $[B_{10}H_8OC(O)C_6H_5(H_2)]^-$ has several isomers. The structure of two of them is represented below. The structure with the boron atom bonded to H_2, located in the same equatorial belt as *exo*-polyhedral substituent, had lower Gibbs energy than the structure where the analogous boron atom was located in the opposite equatorial belt to the *exo*-polyhedral substituent. As in the case of $[B_{10}H_9(H_2)]^-$, one boron atom coordinates the molecule of hydrogen, H_2. The distance between the boron atom and the hydrogen atom was equal to 1.30 Å. The distance between two hydrogen atoms was equal to 0.87 Å.

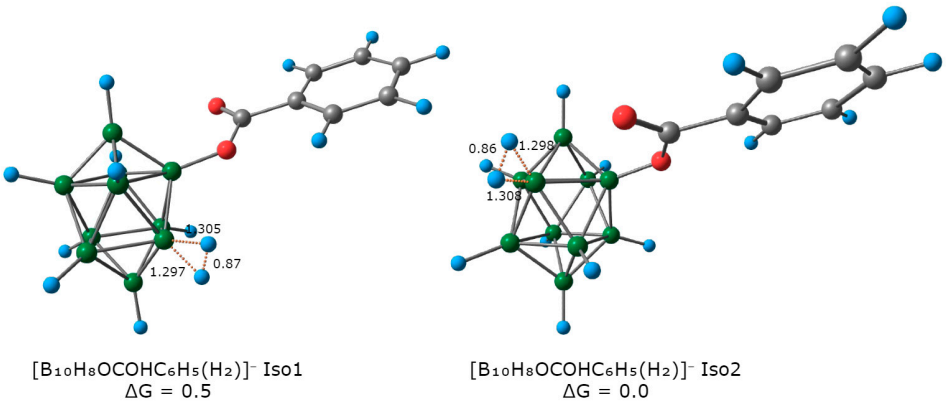

Figure 6. The structure of main isomers of $[B_{10}H_8OC(O)C_6H_5(H_2)]^-$ anion. Length units—Å, energy units—kJ/mol, ωB97X-D3/def2-TZVPP level of theory.

For $[B_{10}H_8OC(O)C_6H_5(H_2)]^-$ systems, QTAIM analysis was performed. As in the case of $[B_{10}H_9(H_2)]^-$, the bond path between the boron atom and the H_2 fragment was indicated. The main descriptors of the electron density at the bcp were very similar to the descriptors in $[B_{10}H_9\_H_2]^-$. The value of $\rho\ (r)$ lay in the range of 0.126 to 0.127 e $Å^{-3}$, the Laplacian of electron density was in the range of 0.342 to 0.350 e $Å^{-5}$, total energy at the bcp was equal to −0.098 to −0.099 h e^{-1} and the delocalization index was equal to 0.335 to 0.344. Thus, it can be concluded that the presence of the *exo*-polyhedral substituent had a slight effect on the nature of B-H_2 interactions.

Then, as in case of $[B_{10}H_9(H_2)]^-$, the H_2 eliminated. For the $[B_{10}H_8OC(O)C_6H_5(H_2)]^-$ isomer, in which the boron atom was bonded to H_2 in the same equatorial belt as the *exo*-polyhedral substituent, the $[B_{10}H_8OC(O)C_6H_5]^-$ molecular specie was localized on the potential energy surface. In the case of the isomer, in which the boron atom was in the opposite equatorial belt to the *exo*-polyhedral substituent, $[B_{10}H_8OC(O)C_6H_5]^-$ was not localized, because the process of geometry optimization led to disubstituted anion $[2,6\text{-}B_{10}H_8O_2CC_6H_5]^-$.

Finally, the process of intramolecular cyclisation occurred, and $[B_{10}H_8O_2CC_6H_5]^-$ was formed (Figure 7). This anion had two isomers. The first isomer $[2,6\text{-}B_{10}H_8O_2CC_6H_5]^-$ had substituted boron atoms in different equatorial belts, whereas the second isomer $[2,3\text{-}B_{10}H_8O_2CC_6H_5]^-$ had two substituted boron atoms in one equatorial belt. The first isomer $[2,6\text{-}B_{10}H_8O_2CC_6H_5]^-$ had significantly lower Gibbs energy than the second isomer $[2,3\text{-}B_{10}H_8O_2CC_6H_5]^-$ (the difference between two isomers is equal to 97.4 kJ/mol). This fact is the reason of high regioselectivity for the formation process of the disubstituted carboxonium derivative. The main geometric parameters of $[2,6\text{-}B_{10}H_8O_2CC_6H_5]^-$ were considered. The B-O bond lengths were equal to 1.535 Å. The C-O bond lengths were equal to 1.269 Å. Obtained parameters were similar to those previously obtained for the $[2,6\text{-}B_{10}H_8O_2CCH_3]^-$ anion.

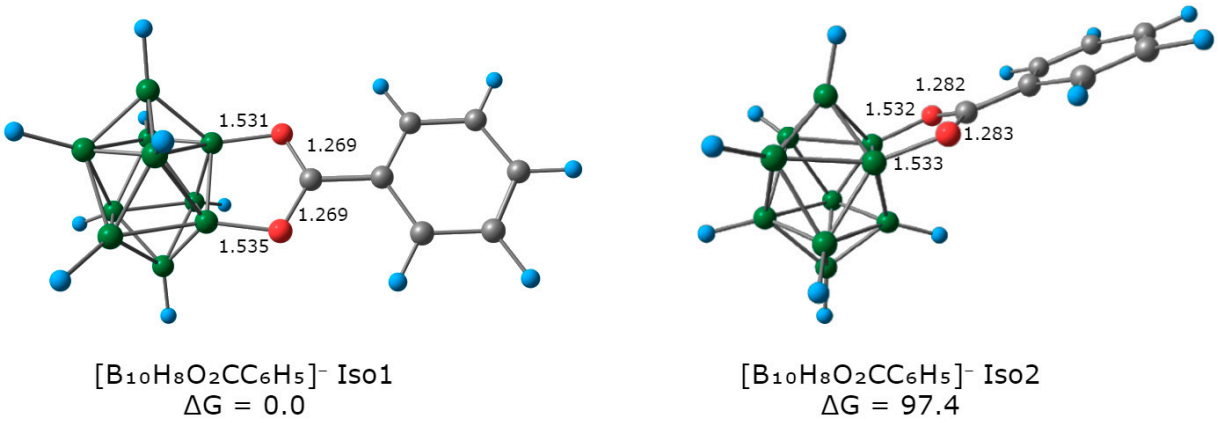

Figure 7. The structure of main isomers of the $[B_{10}H_8O_2CC_6H_5]^-$ anion. Length units—Å; energy units—kJ/mol; ωB97X-D3/def2-TZVPP level of theory.

Thus, the reaction pathway for the formation of $[2,6\text{-}B_{10}H_8O_2CC_6H_5]^-$ was investigated (Scheme 2). This process was based on the EINS mechanism and, as in the case of a previously described analogous process, the key role was played by intermediate anion species in which one boron atom coordinates two hydrogen atoms. The process of $[2,6\text{-}B_{10}H_8O_2CC_6H_5]^-$ formation started with hydrogen migration and the formation of $[B_{10}H_9(H_2)]^-$. Then the H_2 molecule was eliminated, and $[B_{10}H_9]^-$ was formed. The process of H_2 elimination is endergonic, and the ΔG of this process is equal to 49 kJ/mol. Next, $[B_{10}H_9]^-$ interacted with C_6H_5COOH and mono-substituted derivative $[B_{10}H_9OC(OH)C_6H_5]^-$ was formed. This process is quite exergonic and the ΔG of this process is −118 kJ/mol. The proton from the hydroxy-group migrated to the boron cage, with the formation of $[B_{10}H_9OC(O)C_6H_5{*}H^{fac}]^-$. As in the case of $[B_{10}H_{11}]^-$, the proton migrated with the formation of $[B_{10}H_8OC(O)C_6H_5(H_2)]^-$. Finally, the H_2 molecule was eliminated, intermolecular cyclisation occurred and $^-$ was formed. The Gibbs energy of the cyclization process was equal to −162 kJ/mol.

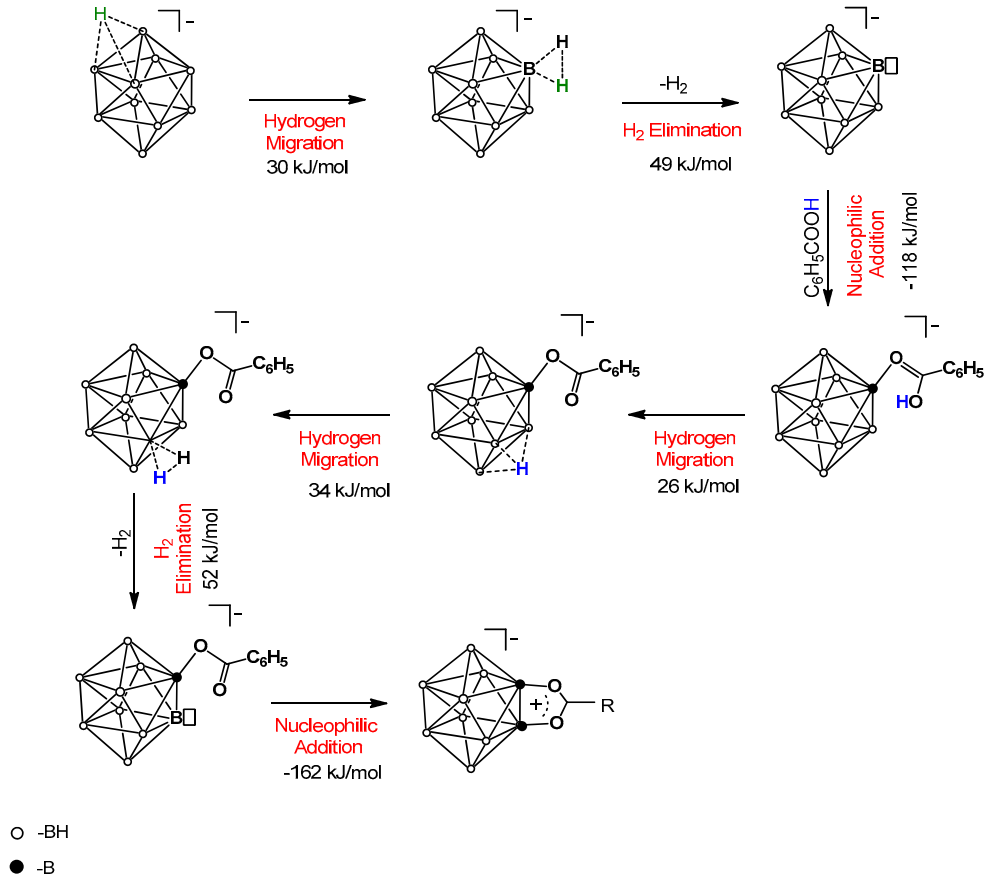

Scheme 2. The general mechanism of $[B_{10}H_8O_2CC_6H_5]^-$ anion formation.

3. Materials and Methods

3.1. IR Spectra

The IR spectra of prepared compounds were recorded on an Infralyum FT 02 Fourier transform spectrometer (Lumex Instruments Research and Production Company, Vancouver, BC, Canada) in the region of 4000 to 300 cm^{-1} and with a resolution of 1 cm^{-1}. Samples were prepared as dichloromethane CH_2Cl_2 solution.

3.2. NMR Spectra

The NMR (^{1}H, 11B, 13C) spectra of solutions of the studied compounds in CD_3CN were recorded on a Bruker (Billerica, MA, USA) Avance II 300 spectrometer operating at 300.3, 96.32 and 75.49 MHz, respectively, using an internal deuterium lock. Tetramethylsilane and Boron trifluoride etherate were used as external references.

3.3. Electrospray Ionisation Mass Spectrometry (ESI-MS)

The LC system consisted of two LC-20AD pumps (Shimadzu, Kyoto, Japan), and an autosampler was coupled online with an LCMS-IT-TOF mass spectrometer equipped with an electrospray ionization source (Shimadzu, Kyoto, Japan). The HRMS spectra were acquired in direct injection mode without column. The samples were prepared as CH3CN solutions. Detection parameters: Detector Voltage 1.55 kV; Nebulising Gas 1.50 L/min; CDL Temperature 200.0 °C.

3.4. X-ray Crystal Structure Determination

The single-crystal X-ray diffraction data for X were collected on a three-circle Bruker D8 Venture diffractometer using φ and ω scan mode. The data were indexed and integrated using the SAINT program (V7.60A) [66] and then scaled and corrected for absorption using the SADABS program (version 2008/1) [67]. For details, see Table S1. The structures were

determined by direct methods and refined by the full-matrix least squares technique on F2 with anisotropic displacement parameters for non-hydrogen atoms. The hydrogen atoms in all compounds were placed in calculated positions and refined within the riding model with fixed isotropic displacement parameters [Uiso(H) = 1.5Ueq(C) for the CH3-groups and 1.2Ueq(C) for the other groups]. All calculations were carried out using the SHELXTL program (version 2018/2) [68] and OLEX2 program package (version 1.5) [69].

Crystallographic data for all investigated compounds have been deposited with the Cambridge Crystallographic Data Centre, CCDC 2,227,408. Copies of this information may be obtained free of charge from the Director, CCDC, 12 Union Road, Cambridge CHB2 1EZ, UK (Fax: +44-1223-336033; e-mail: deposit@ccdc.cam.ac.uk or www.ccdc.cam.ac.uk).

3.5. Computational Details

A complete geometry optimization of all model structures was performed at the ωB97X-D3/def2-TZVPP theory level using the ORCA 4.2.1 software package (the atom-pairwise dispersion correction with the zero-damping scheme was utilized) [70–72]. All calculations were performed using the RIJCOSX approximation with the def2/J auxiliary basis set [73]. Tight criteria of SCF convergence ("Tight SCF") were employed for the calculations. The keywords "Grid5", "FinalGrid6" and "GridX5" were used as parameters for the spatial integration grid. For the model structures with closed electron shells, spin-restricted approximation was utilized. Symmetry operations were not applied during the geometry optimization procedure for all model structures. The Hessian matrices were calculated numerically for all optimized model structures in order to prove the location of correct minima on the potential energy surfaces (no imaginary frequencies for all reactants, intermediates, and final products; only one imaginary frequency for transition states). The connectivity of each reaction step was also confirmed using the intrinsic reaction coordinate (IRC) calculations from the transition states [74–76]. Solvent effects were considered using the Solvation Model based on Density (SMD) [77]. The natural bond orbital (NBO) method was employed, using the NBO7 program package [78,79]. Topological analysis of the electron density distribution, based on the Quantum Theory of Atoms in Molecules (QTAIM) formalism developed by Bader [80,81], was employed with the Multiwfn program (version 3.7) [82]. The Cartesian atomic coordinates for all optimized equilibrium model structures are presented in the Supplementary Materials as the xyz-files. Visualization of the optimized structures was carried out with the help of ChemCraft program version 1.7 [83].

3.6. Materials

Solvents of reagent and special purity grades Sigma-Aldrich (Burlington, MA, USA) and Panreac (Darmstadt, Germany) (99.7%), were used without any additional purification.

3.7. Synthesis of ($(C_4H_9)_4N$)[2,6-$B_{10}H_8O_2CC_6H_5$]

Method A: $((C_4H_9)_4N)[B_{10}H_{11}]$ (0.250 g, 0.69 mmol) and C_6H_5COOH (550 mg, 4.5 mmol) were dissolved in dichloromethane CH_2Cl_2 (10 mL). The resulting mixture was heated in an atmosphere of dry argon at 40 to 43 °C for 12 h. After completion of the reaction process, the solution was cooled to room temperature and the solvent was evaporated using a rotary pump vacuum. The residue was washed with Et_2O (2 × 10 mL) and heated in a vacuum drying oven at 105 °C for 4 h. The product was purified by column chromatography on silica gel, eluting with $CHCl_3/CH_3CN$ mixture (9:1). The yield was 0.240 g (74%) $((C_4H_9)_4N)$[2,6-$B_{10}H_8O_2CC_6H_5$]. IR(CH_2Cl_2.cm^{-1}): 2500 ν(B-H), 1600 ν(C = O). NMR ^{11}B-{^{1}H} (CD_3CN, ppm): 0.3 (s B2, B6, I = 2), −6.6 (d, B1, B10, I = 2), −17.1 (d, B3, B9, I = 2), −29.4 (d, B4, B5, B7, B8, I = 4). NMR ^{1}H (CD_3CN, ppm): 7.98 (d, C_6H_5, I = 2), 7.73 (t, C_6H_5, I = 1), 7.49 (t, C_6H_5, I = 2), 3.05 (t, $(C_4H_9)_4N^+$, I = 8), 1.57 (m, $(C_4H_9)_4N^+$, I = 8), 1.32 (m, $(C_4H_9)_4N^+$, I = 8), 0.93 (t, $(C_4H_9)_4N^+$, I = 12). NMR ^{13}C (CD_3CN, ppm): 184.5 ($O_2CC_6H_5$), 136.6 ($O_2CC_6H_5$), 130.7 ($O_2CC_6H_5$), 129.3 ($O_2CC_6H_5$), 124.5 ($O_2CC_6H_5$), 58.4 ($(C_4H_9)_4N^+$), 23.3 ($(C_4H_9)_4N^+$),

19.4 ($(C_4H_9)_4N^+$), 12.8 ($(C_4H_9)_4N^+$). MS (ESI) m/z: 237.1926 (A refers to the molecular weight of $[B_{10}H_8O_2CC_6H_5]$. Calculated for $\{[A]^-\}$ 237.1924).

Method B: $((C_4H_9)_4N)[B_{10}H_{11}]$ (250 mg, 0.69 mmol) and C_6H_5COOH (550 mg, 4.5 mmol) were dissolved in dichloromethane CH_2Cl_2 (10 mL). The resulting mixture was heated in an autoclave at 75 °C for 4 h. After completion of the reaction process, the solution was cooled to room temperature and the solvent was evaporated using a rotary pump vacuum. The residue was washed with Et_2O (2 × 10 mL) and purified by column chromatography on silica gel, eluting with $CHCl_3/CH_3CN$ mixture (9:1). The yield was 0.255 g (77%) $((C_4H_9)_4N)$[2,6-$B_{10}H_8O_2CC_6H_5$].

4. Conclusions

The process of anion [2,6-$B_{10}H_8O_2CC_6H_5]^-$ preparation was considered both theoretically and experimentally. This process featured the EINS mechanism. The synthesis of the target product was based on the interaction between $[B_{10}H_{11}]^-$ and benzoic acid C_6H_5COOH. The formation of this product proceeded stepwise through the formation of a mono-substituted product $[B_{10}H_9OC(OH)C_6H_5]^-$. The proposed approach is characterized by a simple apparatus configuration and good yields of final products. This approach can be used for synthesis of disubstituted carboxonium derivative with various natures. Using DFT calculations, the main stages of obtaining [2,6-$B_{10}H_8O_2CC_6H_5]^-$ were established. The formation of mono-substituted derivative starts with hydrogen migration and the formation of $[B_{10}H_9(H_2)]^-$. Then the H_2 molecule eliminates and $[B_{10}H_9]^-$ is formed. Next, $[B_{10}H_9]^-$ interacts with C_6H_5COOH and mono-substituted derivative $[B_{10}H_9OC(OH)C_6H_5]^-$ is formed. Then the process of disubstituted product [2,6-$B_{10}H_8O_2CC_6H_5]^-$ formation takes place. A proton from the hydroxy-group of mono-substituted derivatives migrates to the boron cage with the formation of $[B_{10}H_9OC(O)C_6H_5{}^*H^{fac}]^-$. As in the case of $[B_{10}H_{11}]^-$, a proton migrates with the formation of $[B_{10}H_8OC(O)C_6H_5(H_2)]^-$. Finally, the H_2 molecule eliminates, intermolecular cyclisation occurs and [2,6-$B_{10}H_8O_2CC_6H_5]^-$ is formed. Based on the modelling results, the reasons for the regioselectivity of the formation of the target product [2,6-$B_{10}H_8O_2CC_6H_5]^-$ were established.

Supplementary Materials: The following supporting information can be downloaded at: https://www.mdpi.com/article/10.3390/molecules28041757/s1, Figure S1: $^{11}B\{^1H\}$ NMR spectrum of $((C_4H_9)_4N)$[2-$B_{10}H_9OC(OH)C_6H_5$]; Figure S2: $^{11}B\{^1H\}$ NMR spectrum of $((C_4H_9)_4N)[B_{10}H_8O_2CC_6H_5]$. Figure S3: ^1H NMR spectrum of $((C_4H_9)_4N)[B_{10}H_8O_2CC_6H_5]$; Figure S4: ^{13}C-NMR spectrum of $((C_4H_9)_4N)[B_{10}H_8O_2CC_6H_5]$; Figure S5: ESI-MS spectrum of $((C_4H_9)_4N)[B_{10}H_8O_2CC_6H_5]$; Figure S6: IR spectrum of $((C_4H_9)_4N)[B_{10}H_8O_2CC_6H_5]$; Table S1: Crystal data and structure refinement for $((C_4H_9)_4N)[B_{10}H_8O_2CC_6H_5]$; Scheme S1: Extended scheme of preparation of $[B_{10}H_8O_2CC_6H_5]^-$ anion. Figure S7: Contour line map of the electron density for B–(H2) fragment of the $[B_{10}H_9(H_2)]^-$. Figure S8: Molecular graph showing the results of the topological analysis of the electron density distribution in the model structure of the $[B_{10}H_8OCOC_6H_5(H_2)]^-$ isomers; Table S2: Main topological parameters of electron density for B–H_2 interactions; Figure S9: Optimized structure of $[B_{10}H_9]^-$ anion. Figure S10: Optimized structure of $[B_{10}H_8OCOC_6H_5]^-$ anion. Table S3: Cartesian atomic coordinates of the calculated optimized equilibrium model structures.

Author Contributions: Manuscript conception, I.N.K. and A.S.N.; writing and original draft preparation, A.V.K., I.N.K. and A.S.N.; synthesis of derivatives A.V.K. and A.V.N.; NMR analysis, N.A.S. and A.Y.B.; X-ray analysis, A.S.K.; quantum chemical calculations, I.N.K. and A.S.N.; editing, data analysis and interpretation, I.N.K., A.S.N. and A.P.Z.; supervision, K.Y.Z. and N.T.K. All authors have read and agreed to the published version of the manuscript.

Funding: This work was supported by the Russian Science Foundation (project no. 22-73-00201).

Institutional Review Board Statement: Not applicable.

Informed Consent Statement: Not applicable.

Data Availability Statement: Not applicable.

Acknowledgments: A.S.N. is grateful to the RUDN University Strategic Academic Leadership Program (QTAIM analysis and theoretical studies of the structure of intermediate $[B_{10}H_9(H_2)]^-$ with B–(H_2) fragment). This work is prepared in commemoration of the 300th anniversary of St Petersburg State University's founding.

Conflicts of Interest: The authors declare no conflict of interest.

References

1. Adelusi, T.I.; Oyedele, A.-Q.K.; Boyenle, I.D.; Ogunlana, A.T.; Adeyemi, R.O.; Ukachi, C.D.; Idris, M.O.; Olaoba, O.T.; Adedotun, I.O.; Kolawole, O.E.; et al. Molecular modeling in drug discovery. *Inform. Med. Unlocked* **2022**, *29*, 100880. [CrossRef]
2. Gao, K.; Wang, R.; Chen, J.; Cheng, L.; Frishcosy, J.; Huzumi, Y.; Qiu, Y.; Schluckbier, T.; Wei, X.; Wei, G.-W. Methodology-Centered Review of Molecular Modeling, Simulation, and Prediction of SARS-CoV-2. *Chem. Rev.* **2022**, *122*, 11287–11368. [CrossRef] [PubMed]
3. Maurer, R.J.; Freysoldt, C.; Reilly, A.M.; Brandenburg, J.G.; Hofmann, O.T.; Björkman, T.; Lebègue, S.; Tkatchenko, A. Advances in Density-Functional Calculations for Materials Modeling. *Annu. Rev. Mater. Res.* **2019**, *49*, 1–30. [CrossRef]
4. Daniel, C. Density Functional Theories and Coordination Chemistry. In *Reference Module in Chemistry, Molecular Sciences and Chemical Engineering*; Elsevier: Amsterdam, The Netherlands, 2020. [CrossRef]
5. Jones, R.O. Density functional theory: Its origins, rise to prominence, and future. *Rev. Mod. Phys.* **2015**, *87*, 897–923. [CrossRef]
6. Datta, D.; Gordon, M.S. A Massively Parallel Implementation of the CCSD(T) Method Using the Resolution-of-the-Identity Approximation and a Hybrid Distributed/Shared Memory Parallelization Model. *J. Chem. Theory Comput.* **2021**, *17*, 4799–4822. [CrossRef]
7. Rojas, S.; Parravicini, O.; Vettorazzi, M.; Tosso, R.; Garro, A.; Gutiérrez, L.; Andújar, S.; Enriz, R. Combined MD/QTAIM techniques to evaluate ligand-receptor interactions. Scope and limitations. *Eur. J. Med. Chem.* **2020**, *208*, 112792. [CrossRef]
8. Morgante, P.; Peverati, R. The devil in the details: A tutorial review on some undervalued aspects of density functional theory calculations. *Int. J. Quantum Chem.* **2020**, *120*, e26332. [CrossRef]
9. Luo, J.; Dai, H.; Zeng, C.; Wu, D.; Cao, M. A Theoretical Study of the Halogen Bond between Heteronuclear Halogen and Benzene. *Molecules* **2022**, *27*, 8078. [CrossRef]
10. Zhao, L.; Pan, S.; Holzmann, N.; Schwerdtfeger, P.; Frenking, G. Chemical Bonding and Bonding Models of Main-Group Compounds. *Chem. Rev.* **2019**, *119*, 8781–8845. [CrossRef] [PubMed]
11. Kang, P.-L.; Liu, Z.-P. Reaction prediction via atomistic simulation: From quantum mechanics to machine learning. *Iscience* **2020**, *24*, 102013. [CrossRef]
12. Koistinen, O.-P.; Ásgeirsson, V.; Vehtari, A.; Jónsson, H. Minimum Mode Saddle Point Searches Using Gaussian Process Regression with Inverse-Distance Covariance Function. *J. Chem. Theory Comput.* **2019**, *16*, 499–509. [CrossRef] [PubMed]
13. Garcia-Ratés, M.; Neese, F. Effect of the Solute Cavity on the Solvation Energy and its Derivatives within the Framework of the Gaussian Charge Scheme. *J. Comput. Chem.* **2020**, *41*, 922–939. [CrossRef] [PubMed]
14. Ali, H.S.; Ghafoor, S.; de Visser, S.P. Density Functional Theory Study into the Reaction Mechanism of Isonitrile Biosynthesis by the Nonheme Iron Enzyme ScoE. *Top. Catal.* **2022**, *65*, 528–543. [CrossRef]
15. Xie, C.; Sun, Y.; Zhu, B.; Xu, M.; Yu, H.; Liu, E. Density functional theory study on the reaction mechanism of selective catalytic reduction of NO by NH_3 over the γ-Fe2O3 (0 0 1) surface. *Comput. Theor. Chem.* **2020**, *1192*, 113052. [CrossRef]
16. Du, L.; Jin, S.; Nie, P.; She, C.; Wang, J. Initial Decomposition Mechanism of 3-Nitro-1,2,4-triazol-5-one (NTO) under Shock Loading: ReaxFF Parameterization and Molecular Dynamic Study. *Molecules* **2021**, *26*, 4808. [CrossRef]
17. Cortes-Guzman, F.; Bader, R. Complementarity of QTAIM and MO theory in the study of bonding in donor-acceptor complexes. *Coord. Chem. Rev.* **2005**, *249*, 633–662. [CrossRef]
18. Firme, C.L. Local potential energy: A novel QTAIM tool to quantify the binding energy of classical hydrogen bonds. *Chem. Phys. Lett.* **2020**, *754*, 137593. [CrossRef]
19. Alikhani, M.E. On the chemical bonding features in boron containing compounds: A combined QTAIM/ELF topological analysis. *Phys. Chem. Chem. Phys.* **2013**, *15*, 12602–12609. [CrossRef]
20. Lepetit, C.; Fau, P.; Fajerwerg, K.; Kahn, M.L.; Silvi, B. Topological analysis of the metal-metal bond: A tutorial review. *Coord. Chem. Rev.* **2017**, *345*, 150–181. [CrossRef]
21. Jacobsen, H. Chemical bonding in view of electron charge density and kinetic energy density descriptors. *J. Comput. Chem.* **2009**, *30*, 1093–1102. [CrossRef] [PubMed]
22. Geerlings, P.; Chamorro, E.; Chattaraj, P.K.; De Proft, F.; Gázquez, J.L.; Liu, S.; Morell, C.; Toro-Labbé, A.; Vela, A.; Ayers, P. Conceptual density functional theory: Status, prospects, issues. *Theor. Chem. Accounts* **2020**, *139*, 36. [CrossRef]
23. Domingo, L.R.; Ríos-Gutiérrez, M.; Pérez, P. Applications of the Conceptual Density Functional Theory Indices to Organic Chemistry Reactivity. *Molecules* **2016**, *21*, 748. [CrossRef]
24. Huang, Y.; Rong, C.; Zhang, R.; Liu, S. Evaluating frontier orbital energy and HOMO/LUMO gap with descriptors from density functional reactivity theory. *J. Mol. Model.* **2017**, *23*, 3. [CrossRef]
25. Chattaraj, P.K.; Giri, S. Electrophilicity index within a conceptual DFT framework. *Annu. Rep. Prog. Chem. Sect. C* **2009**, *105*, 13–39. [CrossRef]

26. Chakraborty, D.; Chattaraj, P.K. Conceptual density functional theory based electronic structure principles. *Chem. Sci.* **2021**, *12*, 6264–6279. [CrossRef] [PubMed]
27. Qin, X.-F.; Wu, H.-S.; Jiao, H. Structures and aromaticity of closo-$B_nH_{n-1}CO^-$ (n=5 − 12). *J. Mol. Struct. THEOCHEM* **2007**, *822*, 111–115. [CrossRef]
28. Sethio, D.; Daku, L.M.L.; Hagemann, H.; Kraka, E. Quantitative Assessment of B−B−B, B−H_b−B, and B−H_t Bonds: From BH_3 to $B_{12}H_{12}{}^{2-}$. *ChemPhysChem* **2019**, *20*, 1967–1977. [CrossRef] [PubMed]
29. Tu, D.; Yan, H.; Poater, J.; Solà, M. The *nido*-Cage···π Bond: A Non-covalent Interaction between Boron Clusters and Aromatic Rings and Its Applications. *Angew. Chem. Int. Ed.* **2020**, *59*, 9018–9025. [CrossRef]
30. Piña, M.D.L.N.; Bauzá, A.; Frontera, A. Halogen···halogen interactions in decahalo-*closo*-carboranes: CSD analysis and theoretical study. *Phys. Chem. Chem. Phys.* **2020**, *22*, 6122–6130. [CrossRef] [PubMed]
31. Avdeeva, V.; Malinina, E.; Kuznetsov, N. Boron cluster anions and their derivatives in complexation reactions. *Coord. Chem. Rev.* **2022**, *469*, 214636. [CrossRef]
32. Zhao, X.; Yang, Z.; Chen, H.; Wang, Z.; Zhou, X.; Zhang, H. Progress in three-dimensional aromatic-like closo-dodecaborate. *Coord. Chem. Rev.* **2021**, *444*, 214042. [CrossRef]
33. Stogniy, M.Y.; Erokhina, S.A.; Sivaev, I.B.; Bregadze, V.I. Nitrilium derivatives of polyhedral boron compounds (boranes, carboranes, metallocarboranes): Synthesis and reactivity. *Phosphorus Sulfur Silicon Relat. Elem.* **2019**, *194*, 983–988. [CrossRef]
34. Bogdanova, E.V.; Stogniy, M.Y.; Chekulaeva, L.A.; Anisimov, A.A.; Suponitsky, K.Y.; Sivaev, I.B.; Grin, M.A.; Mironov, A.F.; Bregadze, V.I. Synthesis and reactivity of propionitrilium derivatives of cobalt and iron bis(dicarbollides). *New J. Chem.* **2020**, *44*, 15836–15848. [CrossRef]
35. Semioshkin, A.A.; Sivaev, I.B.; Bregadze, V.I. Cyclic oxonium derivatives of polyhedral boron hydrides and their synthetic applications. *Dalton Trans.* **2008**, *11*, 977–992. [CrossRef] [PubMed]
36. Semioshkin, A.; Bregadze, V.; Godovikov, I.; Ilinova, A.; Laskova, J.; Starikova, Z. Synthesis and structure of 1-iodo-7-dioxonium-decahydro-closo-dodecaborate. *J. Organomet. Chem.* **2011**, *696*, 2760–2762. [CrossRef]
37. Stogniy, M.Y.; Bogdanova, E.V.; Anufriev, S.A.; Sivaev, I.B. Synthesis of New Rhodacarborane [3,3-(1′,5′-COD)-8-PrNH=C(Et)NH-3,1,2-$RhC_2B_9H_{10}$]. *Russ. J. Inorg. Chem.* **2022**, *67*, 1537–1544. [CrossRef]
38. Laskova, J.; Ananiev, I.; Kosenko, I.; Serdyukov, A.; Stogniy, M.; Sivaev, I.; Grin, M.; Semioshkin, A.; Bregadze, V.I. Nucleophilic addition reactions to nitrilium derivatives $[B_{12}H_{11}NCCH_3]^-$ and $[B_{12}H_{11}NCCH_2CH_3]^-$. Synthesis and structures of *closo*-dodecaborate-based iminols, amides and amidines. *Dalton Trans.* **2022**, *51*, 3051–3059. [CrossRef] [PubMed]
39. Avdeeva, V.V.; Garaev, T.M.; Malinina, E.A.; Zhizhin, K.Y.; Kuznetsov, N.T. Physiologically Active Compounds Based on Membranotropic Cage Carriers–Derivatives of Adamantane and Polyhedral Boron Clusters (Review). *Russ. J. Inorg. Chem.* **2022**, *67*, 28–47. [CrossRef]
40. Zhu, T.-C.; Xing, Y.-Y.; Sun, Y.; Duttwyler, S.; Hong, X. Directed B–H functionalization of the *closo*-dodecaborate cluster via concerted iodination–deprotonation: Reaction mechanism and origins of regioselectivity. *Org. Chem. Front.* **2020**, *7*, 3648–3655. [CrossRef]
41. Zhdanov, A.; Zhdanova, K.; Bykov, A.; Kochnev, V.; Grigoriev, M.; Zhizhin, K.; Kuznetsov, N. Selective synthesis of the $[2\text{-}B_{10}H_9I]^{2-}$ anion and some theoretical aspects of its iodination process. *Polyhedron* **2018**, *139*, 125–130. [CrossRef]
42. Kochnev, V.K.; Kuznetsov, N.T. Theoretical study of protonation of the $B_{10}H_{10}{}^{2-}$ anion and subsequent hydrogen removal due to substitution reaction in acidic medium. *Comput. Theor. Chem.* **2016**, *1075*, 77–81. [CrossRef]
43. Klyukin, I.; Vlasova, Y.; Novikov, A.; Zhdanov, A.; Zhizhin, K.; Kuznetsov, N. Theoretical Study of *closo*-Borate Anions $[B_nH_n]^{2-}$ (n = 5–12): Bonding, Atomic Charges, and Reactivity Analysis. *Symmetry* **2021**, *13*, 464. [CrossRef]
44. Klyukin, I.N.; Vlasova, Y.S.; Novikov, A.S.; Zhdanov, A.P.; Hagemann, H.R.; Zhizhin, K.Y.; Kuznetsov, N.T. B-F bonding and reactivity analysis of mono- and perfluoro-substituted derivatives of closo-borate anions (6, 10, 12): A computational study. *Polyhedron* **2022**, *211*, 115559. [CrossRef]
45. Bolotin, D.S.; Burianova, V.K.; Novikov, A.S.; Demakova, M.Y.; Pretorius, C.; Mokolokolo, P.P.; Roodt, A.; Bokach, N.A.; Suslonov, V.V.; Zhdanov, A.P.; et al. Nucleophilicity of Oximes Based upon Addition to a Nitrilium *closo*-Decaborate Cluster. *Organometallics* **2016**, *35*, 3612–3623. [CrossRef]
46. Nelyubin, A.V.; Selivanov, N.A.; Bykov, A.Y.; Klyukin, I.N.; Novikov, A.S.; Zhdanov, A.P.; Karpechenko, N.Y.; Grigoriev, M.S.; Zhizhin, K.Y.; Kuznetsov, N.T. Primary Amine Nucleophilic Addition to Nitrilium *Closo*-Dodecaborate $[B_{12}H_{11}NCCH_3]^-$: A Simple and Effective Route to the New BNCT Drug Design. *Int. J. Mol. Sci.* **2021**, *22*, 13391. [CrossRef]
47. Jelinek, T.; Štibr, B.; Mareš, F.; Plešek, J.; Heřmánek, S. Halogenation of 4,5-dicarba-arachno- nonaborane(13),4,5-$C_2B_7H_{13}$. *Polyhedron* **1987**, *6*, 1737–1740. [CrossRef]
48. Frank, R.; Adhikari, A.K.; Auer, H.; Hey-Hawkins, E. Electrophile-Induced Nucleophilic Substitution of the *nido*-Dicarbaundecaborate Anion*nido*-7,8-$C_2B_9H_{12}{}^-$by Conjugated Heterodienes. *Chem. A Eur. J.* **2013**, *20*, 1440–1446. [CrossRef] [PubMed]
49. Laila, Z.; Yazbeck, O.; Ghaida, F.A.; Diab, M.; El Anwar, S.; Srour, M.; Mehdi, A.; Naoufal, D. Clean-activation of the B–H bond in closo-decahydrodecaborate $[B_{10}H_{10}]^{2-}$ anion via soft-route. *J. Organomet. Chem.* **2020**, *910*, 121132. [CrossRef]
50. Mahfouz, N.; Ghaida, F.A.; El Hajj, Z.; Diab, M.; Floquet, S.; Mehdi, A.; Naoufal, D. Recent Achievements on Functionalization within closo-Decahydrodecaborate $[B_{10}H_{10}]^{2-}$ Clusters. *Chemistryselect* **2022**, *7*, e202200770. [CrossRef]

51. Peymann, T.; Lork, E.; Gabel, D. Hydroxoundecahydro-closo-dodecaborate (2−) as a Nucleophile. Preparation and Structural Characterization of O-Alkyl and O-Acyl Derivatives of Hydroxoundecahydro-closo-dodecaborate (2−). *Inorg. Chem.* **1996**, *35*, 1355–1360. [CrossRef]
52. Kubasov, A.; Turishev, E.; Kopytin, A.; Shpigun, L.; Zhizhin, K.; Kuznetsov, N. Sulfonium closo-hydridodecaborate anions as active components of a potentiometric membrane sensor for lidocaine hydrochloride. *Inorg. Chim. Acta* **2020**, *514*, 119992. [CrossRef]
53. Kubasov, A.S.; Turyshev, E.S.; Novikov, I.V.; Gurova, O.M.; Starodubets, P.A.; Golubev, A.V.; Zhizhin, K.Y.; Kuznetsov, N.T. Theoretical and experimental comparison of the reactivity of the sulfanyl-closo-decaborate and sulfanyl-closo-dodecaborate anions and their mono-S-substituted derivatives. *Polyhedron* **2021**, *206*, 115347. [CrossRef]
54. Golub, I.; Filippov, O.; Belkova, N.; Epstein, L.; Shubina, E. The Reaction of Hydrogen Halides with Tetrahydroborate Anion and Hexahydro-*closo*-hexaborate Dianion. *Molecules* **2021**, *26*, 3754. [CrossRef] [PubMed]
55. Golub, I.E.; Filippov, O.A.; Belkova, N.V.; Epstein, L.M.; Shubina, E.S. The Mechanism of Halogenation of Decahydro-closo-Decaborate Dianion by Hydrogen Chloride. *Russ. J. Inorg. Chem.* **2021**, *66*, 1639–1648. [CrossRef]
56. Kochnev, V.K.; Avdeeva, V.V.; Malinina, E.A.; Kuznetsov, N.T. Theoretical study of molecular hydrogen elimination from the undecahydrodecaborate monoanion $[B_{10}H_{11}]^-$. Exopolyhedral substitution intermediates: $[B10H9]^-$ monoanion and neutral $[B_{10}H_{10}]$ cluster. *Russ. J. Inorg. Chem.* **2014**, *59*, 706–712. [CrossRef]
57. Cao, K.; Zhang, C.-Y.; Xu, T.-T.; Wu, J.; Wen, X.-Y.; Jiang, W.-J.; Chen, M.; Yang, J. Synthesis of Polyhedral Borane Cluster Fused Heterocycles via Transition Metal Catalyzed B-H Activation. *Molecules* **2020**, *25*, 391. [CrossRef]
58. Klyukin, I.N.; Zhdanov, A.P.; Bykov, A.Y.; Razgonyaeva, G.A.; Grigor'ev, M.S.; Zhizhin, K.Y.; Kuznetsov, N.T. A new method for the synthesis of carboxonium derivatives of the closo-decaborate anion $[2,6\text{-}B10H8(O2CR)]^-$, where R = CH_3, C_2H_5. *Russ. J. Inorg. Chem.* **2017**, *62*, 1479–1482. [CrossRef]
59. Safronova, E.F.; Avdeeva, V.V.; Polyakova, I.N.; Vologzhanina, A.V.; Goeva, L.V.; Malinina, E.A.; Kuznetsov, N.T. Synthesis and Structure of Disubstituted Closo-Decaborate Anion Derivatives $Ph_4P(2,6\text{-}B_{10}H_8O_2CCH_3)$ and $1,2\text{-}B_{10}H_8$Phen with Bifunctional O,O′- and N,N′-Substituents. In *Doklady Chemistry*; Springer: New York, NY, USA, 2013; Volume 452, pp. 240–244. [CrossRef]
60. Klyukin, I.; Zhdanov, A.; Matveev, E.; Razgonyaeva, G.; Grigoriev, M.; Zhizhin, K.; Kuznetsov, N. Synthesis and reactivity of closo-decaborate anion derivatives with multiple carbon–oxygen bonds. *Inorg. Chem. Commun.* **2014**, *50*, 28–30. [CrossRef]
61. Klyukin, I.N.; Kolbunova, A.V.; Novikov, A.S.; Nelyubin, A.V.; Selivanov, N.A.; Bykov, A.Y.; Klyukina, A.A.; Zhdanov, A.P.; Zhizhin, K.Y.; Kuznetsov, N.T. Protonation of Borylated Carboxonium Derivative $[2,6\text{-}B_{10}H_8O_2CCH_3]^-$: Theoretical and Experimental Investigation. *Int. J. Mol. Sci.* **2022**, *23*, 4190. [CrossRef]
62. Nikolova, V.; Cheshmedzhieva, D.; Ilieva, S.; Galabov, B. Atomic Charges in Describing Properties of Aromatic Molecules. *J. Org. Chem.* **2019**, *84*, 1908–1915. [CrossRef]
63. Oller, J.; Pérez, P.; Ayers, P.W.; Vöhringer-Martinez, E. Global and local reactivity descriptors based on quadratic and linear energy models for α,β-unsaturated organic compounds. *Int. J. Quantum Chem.* **2018**, *118*, e25706. [CrossRef]
64. Zhang, K.; Chen, L.; Geng, D.; Lu, J.; Wu, J. Thermal stability mechanism via energy absorption by chemical bonds bending and stretching in free space and the interlayer reaction of layered molecular structure explosives. *Phys. Chem. Chem. Phys.* **2020**, *22*, 13248–13260. [CrossRef]
65. Nelyubin, A.V.; Klyukin, I.N.; Novikov, A.S.; Zhdanov, A.P.; Selivanov, N.A.; Bykov, A.Y.; Kubasov, A.S.; Zhizhin, K.Y.; Kuznetsov, N.T. New Aspects of the Synthesis of closo-Dodecaborate Nitrilium Derivatives $[B_{12}H_{11}NCR]^-$; (R = n-C_3H_7, i-C_3H_7, 4-$C_6H_4CH_3$, 1-$C_{10}H_7$): Experimental and Theoretical Studies. *Inorganics* **2022**, *10*, 196. [CrossRef]
66. *Bruker, SAINT*; Bruker AXS Inc.: Madison, WI, USA, 2018.
67. Krause, L.; Herbst-Irmer, R.; Sheldrick, G.M.; Stalke, D. Comparison of silver and molybdenum microfocus X-ray sources for single-crystal structure determination. *J. Appl. Crystallogr.* **2015**, *48*, 3–10. [CrossRef]
68. Sheldrick, G.M. *SHELXT*—Integrated space-group and crystal-structure determination. *Acta Crystallogr. Sect. A Found. Adv.* **2015**, *71*, 3–8. [CrossRef] [PubMed]
69. Dolomanov, O.V.; Bourhis, L.J.; Gildea, R.J.; Howard, J.A.K.; Puschmann, H. OLEX2: A complete structure solution, refinement and analysis program. *J. Appl. Cryst.* **2009**, *42*, 339–341. [CrossRef]
70. Neese, F. The ORCA program system. *Wiley Interdiscip. Rev. Comput. Mol. Sci.* **2012**, *2*, 73–78. [CrossRef]
71. Grimme, S.; Antony, J.; Ehrlich, S.; Krieg, H. A consistent and accurate ab initio parametrization of density functional dispersion correction (DFT-D) for the 94 elements H-Pu. *J. Chem. Phys.* **2010**, *132*, 154104–154119. [CrossRef] [PubMed]
72. Weigend, F.; Ahlrichs, R. Balanced basis sets of split valence, triple zeta valence and quadruple zeta valence quality for H to Rn: Design and assessment of accuracy. *Phys. Chem. Chem. Phys.* **2005**, *7*, 3297–3305. [CrossRef] [PubMed]
73. Weigend, F. Accurate Coulomb-fitting basis sets for H to Rn. *Phys. Chem. Chem. Phys.* **2006**, *8*, 1057–1065. [CrossRef]
74. Gonzalez, C.; Schlegel, H.B. An improved algorithm for reaction path following. *J. Chem. Phys.* **1989**, *90*, 2154–2161. [CrossRef]
75. Gonzalez, C.; Schlegel, H.B. Reaction path following in mass-weighted internal coordinates. *J. Phys. Chem.* **1990**, *94*, 5523–5527. [CrossRef]
76. Gonzalez, C.; Schlegel, H.B. Improved algorithms for reaction path following: Higher-order implicit algorithms. *J. Chem. Phys.* **1991**, *95*, 5853–5860. [CrossRef]

77. Marenich, A.V.; Cramer, C.J.; Truhlar, D.G. Universal Solvation Model Based on Solute Electron Density and on a Continuum Model of the Solvent Defined by the Bulk Dielectric Constant and Atomic Surface Tensions. *J. Phys. Chem. B* **2009**, *113*, 6378–6396. [CrossRef] [PubMed]
78. Glendening, E.D.; Landis, C.R.; Weinhold, F. *NBO 7.0*: New vistas in localized and delocalized chemical bonding theory. *J. Comput. Chem.* **2019**, *40*, 2234–2241. [CrossRef]
79. Glendening, J.K.; Badenhoop, A.E.R.; Carpenter, J.A.; Bohmann, C.M.; Morales, P.K.; Landis, C.R.; Weinhold, F. *NBO 7.0*; University of Wisconsin: Madison, WI, USA, 2018.
80. Bader, R.F.W. *Atoms in Molecules: A Quantum Theory*; Oxford University Press: Oxford, UK, 1990.
81. Bader, R.F.W.; Legare, D.A. Properties of atoms in molecules: Structures and reactivities of boranes and carboranes. *Can. J. Chem.* **1992**, *70*, 657–677. [CrossRef]
82. Lu, T.; Chen, F. Multiwfn: A multifunctional wavefunction analyzer. *J. Comput. Chem.* **2011**, *33*, 580–592. [CrossRef]
83. Chemcraft—Graphical Software for Visualization of Quantum Chemistry Computations. Available online: https://www.chemcraftprog.com (accessed on 23 January 2023).

Disclaimer/Publisher's Note: The statements, opinions and data contained in all publications are solely those of the individual author(s) and contributor(s) and not of MDPI and/or the editor(s). MDPI and/or the editor(s) disclaim responsibility for any injury to people or property resulting from any ideas, methods, instructions or products referred to in the content.